UNIVERSITY OF PORTSMOUTH

US AFSOR Study Report

The effects of LCF loadings on HCF crack growth

Final Report for Phase III

F569

Submitted by:

R.F. Hall, B.E. Powell and J.Byrne

October 2000

MECHANICAL BEHAVIOUR OF MATERIALS LABORATORY

DEPARTMENT OF MECHANICAL AND MANUFACTURING ENGINEERING

Anglesea Building, Anglesea Road
Portsmouth PO1 3DJ

Phone: +44 (0)23 92 842370 E-mail: jim.byrne@port.ac.uk
Phone: +44 (0)23 92 842325 E-mail: rod.hall@port.ac.uk
Fax: +44 (0)23 92 842351

UNIVERSITY OF PORTSMOUTH

US AFSOR Study Report

The effects of LCF loadings on HCF crack growth

Final Report for Phase III

F569

Submitted by:

R.F. Hall, B.E. Powell and J.Byrne

October 2000

MECHANICAL BEHAVIOUR OF MATERIALS LABORATORY

DEPARTMENT OF MECHANICAL AND MANUFACTURING ENGINEERING

Anglesea Building, Anglesea Road
Portsmouth PO1 3DJ

Phone: +44 (0)23 92 842370 E-mail: jim.byrne@port.ac.uk
Phone: +44 (0)23 92 842325 E-mail: rod.hall@port.ac.uk
Fax: +44 (0)23 92 842351

THE EFFECT OF LCF LOADINGS ON HCF CRACK GROWTH

REPORT FOR THE PERIOD AUG UST 1999 – AUGUST 2000

REPORT NO F 569

NOTATION

DCPD	direct current potential difference
FCG	fatigue crack growth
FOD	foreign object damage
HCF	high cycle fatigue
LCF	low cycle fatigue
MOC	multiple overload cycles: a type of HCF + LCF loading
MUC	multiple underload cycles: a type of HCF + LCF loading
SOC	single overload cycle: a type of HCF + LCF loading
SUC	single underload cycle: a type of HCF + LCF loading
da/dN_{HCF}	crack growth increment resulting from the application of a HCF cycle
da/dN_{LCF}	crack growth increment resulting from the application of a LCF cycle
da/dB	crack growth increment resulting from the application of a HCF + LCF loading block
da/dB_{HCF}	crack growth increment resulting from the application of the HCF cycles within a loading block
da/dB_{LCF}	crack growth increment resulting from the application of the LCF cycles within a loading block
ΔK, DK	stress intensity range
ΔK_{HCF}	stress intensity range associated with a HCF cycle
ΔK_{LCF}	stress intensity range associated with a LCF cycle, i.e. the peak-to-peak load cycle
$\Delta K_{HCF.onset}$	the value of ΔK_{HCF} associated with the onset of HCF crack growth
$\Delta K_{LCF.onset}$	the value of ΔK_{LCF} associated with the onset of HCF crack growth
ΔK_{th}	threshold value of stress intensity range
$K_{max.th}$	threshold value of maximum stress intensity
$\sigma_{max,HCF}$	maximum HCF stress
$\sigma_{min,HCF}$	minimum HCF stress
$\sigma_{max,LCF}$	maximum LCF stress
$\sigma_{min,LCF}$	minimum LCF stress
N_{HCF}	number of HCF cycles in a loading block
N_{LCF}	number of LCF cycles in a loading block
n	ratio N_{HCF} : N_{LCF}
R_{HCF}	stress ratio of the HCF cycles
R_{LCF}	stress ratio of the LCF cycles
s	seconds
T	overload ratio; i.e. the maximum LCF stress / maximum HCF stress.
W	Wheeler constant

1. INTRODUCTION

Continuing service failures in aero-engines and the increased use of ageing aircraft have highlighted the limitations in the current technical and fundamental understanding of the fatigue integrity of engineering components. There is at present insufficient guidance to enable an engineer to account for the reduced high cycle fatigue (HCF) life consequent upon various forms and amounts of damage, such as low cycle fatigue (LCF), foreign object damage (FOD), corrosion, fretting etc., each of which promotes crack initiation, thereby compromising the HCF life. Thus it is that the US Secretary for Defence has declared that: "HCF is the number one readiness issue in the USAF". It is known for example that galling and fretting can reduce the HCF strength of titanium alloys by 80 and 60 % respectively. The two major concerns however are FOD and the complexity of the interactions between LCF and HCF. The second technical challenge is to incorporate non-destructive evaluation as an element of fatigue management. The concern here will always be to characterise the largest defect that is not detected in large structures and complex systems where inspectability may be difficult.

As a consequence, the present work is concerned to measure and model the fatigue crack growth rates associated with HCF loadings, particularly as they are affected by the presence of different proportions of LCF induced fatigue crack growth. The threshold values for HCF crack growth, both in the presence and absence of LCF crack growth, are studied, since they may be used to calculate critical crack sizes for components and structures subjected to HCF stress cycles.

2. EXPERIMENTAL DETAILS

The material selected for testing is Ti-6Al-4V. This is the most widely used titanium alloy, and it is extensively employed in the construction of aero-engine fans and compressors. Test pieces have been supplied by Rolls-Royce plc and were all cut

from engine disc forgings that had been solution-treated and overaged. In this forged condition, the microstructure contained 47% primary alpha phase by volume, in the form of particles which were typically 45 μm long and 15 μm wide. The matrix of transformed beta consisted of colonies of aligned alpha separated by thin beta laminations, with an average colony width of 15 μm. Typical values of the room temperature tensile strength, proof stress and reduction in area exhibited by the material were 960 MPa, 860 MPa and 35%, respectively.

Corner notched testpieces having a 10 x 10 or 7 x 7 mm square cross-section at their gauge length have been cut from a Ti-6Al-4V disc. The specimen orientation, as defined by ASTM notation [**1**] was longitudinal - short transverse (LS) which corresponded to the growth of a crack through the thickness of a fan blade in response to centrifugally induced stresses.

The specimens have been cyclically loaded in a special test facility which combines an electromagnetic vibrator with a servo-hydraulic fatigue machine. This hybrid machine could therefore apply HCF cycles and LCF cycles either separately or conjointly. Figures **1** and **2** are schematic representations of the four HCF+LCF and the jump-in threshold loading patterns used in the tests. The HCF cycles in the HCF+LCF loading blocks are preceded by: a single underload cycle, multiple underload cycles, a single overload cycle, and multiple overload cycles. Consequently these loading blocks will be identified by the abbreviations: SUC, MUC, SOC, and MOC, respectively. The HCF cycles were sinusoidal stress waves with a frequency of 157 Hz. The LCF cycles were trapezoidal stress waves with 1s rise and fall times and a stress ratio of 0.01. The overload ratio is given by the maximum LCF stress/maximum HCF stress.

The fatigue crack growth rates resulting from the repeated application of various combinations of HCF and LCF cycles have been measured, with duplicate tests being undertaken for each loading pattern. Each specimen was

precracked at room temperature in order to generate a near-quarter circular crack with a radius of not less than 0.6 mm. The final loads for the precracking were equal to, or less than, the loads to be used in testing. After the end of precracking, the length of the crack in the specimen was determined with the aid of acetate replicas. For testing, a pulsed direct current potential difference system (DCPD) was used to monitor the crack growth as a function of the number of applied cycles or loading blocks; the output of the system being the ratio of the voltage across the mouth of the crack to that across reference probes placed remotely but within the gauge length of the specimen. Each experiment was terminated at a crack length of approximately half the specimen width and, following the breaking open of the specimen, the final crack length was determined using an optical microscope.

The test data was analysed by the three-point secant method; the input data consisting of paired values of voltage ratio and either cycles or loading blocks corresponding to equal increments in the voltage ratio. This procedure resulted in a ratio of crack increment to crack length measuring precision of 20. The linear relationship between voltage ratio and crack length established by Hicks and Pickard [**2**], defined by the known values of voltage ratio and crack length measured at the start and end of the test, provided the calibration for the crack length monitoring system. The ranges of stress intensity factor associated with the HCF and LCF cycles were calculated using Pickard's [**3**] solution for the free surface position of a quarter-circular crack growing under remote tension.

No previous work on Ti-6Al-4V has suggested any interaction between HCF and LCF cycles at the stress intensities employed in the current work. Hence FCG rates for HCF cycles were calculated by subtraction of the FCG rates due to LCF cycles from the FCG rates from HCF+LCF loading blocks. The relationship between ΔK_{HCF} and ΔK_{LCF} where no overloads are present is :-

$$\Delta K_{HCF} = \Delta K_{LCF} \times (1 - R_{HCF}) / (1 - R_{LCF}) \qquad (1)$$

In addition, the fatigue threshold values associated with a step-change from LCF to HCF loadings were determined. The crack was first grown at a stress ratio of 0.01, and then the HCF loading with the required stress ratio of 0.7, 0.8 or 0.9 applied. The maximum applied LCF stress was equal to the maximum applied HCF stress.

Crack growth rates calculated on a small number of cycles are unreliable, so although the crack growth rate was monitored all through cycling, threshold was calculated on the crack extension over 1 million plus HCF cycles. After 1 million HCF cycles the crack growth rate was tested in relation to the accepted threshold FCG rate of $1x10^{-8}$ mm/cycle. If the threshold value had not been exceeded, further LCF cycles at a stress ratio of 0.01 were applied to extend the crack and consequently increase ΔK, before returning to cycles at the same HCF loads as before. If the crack growth rate exceeded the accepted threshold value, the test was terminated.

During testing all crack lengths were estimated from the DCPD voltage ratio using data derived from previous tests. When the crack had extended half-way through, the specimen was broken open and the actual crack lengths measured. Using these lengths, corrections were then made to the stored values of FCG rates and of ΔK. The corrected data was inspected for FCG rates of $1x10^{-8}$ mm/cycle and the spread of ΔK over which these occurred have been quoted as the range of ΔK_{th}.

This report contains the results from outstanding HCF+LCF tests using SUC and SOC as presented in Table 1, where the overload ratio, T is given by the maximum LCF stress/maximum HCF stress. Threshold tests have been completed and the results analysed. for $R_{HCF} = 0.7$ and 0.9. In addition, the data from threshold tests for $R_{HCF} = 0.8$ has been re-assessed to ensure data for all three values of R_{HCF} are comparable.

Table 1 Summary of all stress ratios and overload ratios at which single underload and single overload HCF+LCF tests, with a cycle ratio of 1000:1, have been completed.

Overload Ratio	Stress Ratio		
	$R_{HCF} = 0.7$	$R_{HCF} = 0.8$	$R_{HCF} = 0.9$
SUC, T = 1.0	√	√	√
SOC, T = 1.15	√	√	
SOC, T = 1.3	√	√	√
SOC, T = 1.45	√	√	

Data from all HCF+LCF tests in the table have been collected together and are presented in this report.

3 RESULTS

3.1 Combined HCF + LCF

For HCF + LCF tests with a stress ratio, R_{HCF} of 0.7, results from tests with single underload cycles, and single overload cycles with an overload ratio of 1.3, have been presented previously [4]. In this report, the data for overload ratios of 1.15 and 1.45 are presented. For these tests, the applied stresses in relation to Figure 1 were those set out in Table 2. A cycle ratio of 1000:1 has been used throughout the data presented in this report.

Table 2 Stresses applied during tests at $R_{HCF} = 0.7$, the results of which are presented in this report. Stress numbers refer to Figure 1 and all values are MPa.

	T = 1.15	T = 1.45
Stress 1	287.5	362.5
Stress 2	250	250
Stress 3	175	175
Stress 4	2.9	3.6

Figure 3 presents the analysed test data for an overload ratio of 1.15. Data from the two tests are in good agreement and a second order polynomial fit has been constructed through the data as shown in Figure 4. The polynomial curve intersects the curve representing the FCG rate from LCF only cycles [4] at a value of ΔK_{LCF} = 10.8 MPa$\sqrt{m}$.

Figure 5 shows the analysed test data for an overload ratio of 1.45. Again the two sets of data are in good agreement and a second order polynomial is fitted through the data, Figure 6. The polynomial curve intersects the LCF data at ΔK_{LCF} = 13.0 MPa$\sqrt{m}$.

For a stress ratio, R_{HCF} of 0.9, single underload cycle, and tests with a single overload cycles at an overload ratio of 1.3 have been undertaken, as detailed in Table 3.

Table 3 Stresses applied during tests at R_{HCF} == 0.9, the results of which are presented in this report. Stress numbers refer to Figure 1 and all values are MPa.

	SUC T=1.0	T = 1.3
Stress 1	250	325
Stress 2	250	250
Stress 3	225	225
Stress 4	2.5	3.2

The results from the two SUC tests are presented in Figure 7. The data are in general agreement and are located closer to the LCF curve than data from tests at R_{HCF}=0.7. A second order polynomial fit has been made to the test data, Figure 8, ignoring the early, often unreliable, results from one test. The polynomial and LCF curves intersect at ΔK_{LCF} = 15.1 MPa$\sqrt{m}$.

Similarly Figures 9 and 10 illustrate the results from the two SOC tests at T = 1.3 where the fitted polynomial curve intersects the LCF data at ΔK_{LCF}=18.2 MPa$\sqrt{m}$. It is not proposed to undertake HCF+LCF tests at T=1.15 and T=1.45 as it is a reasonable assumption that the trends established for R_{HCF}=0.7 and 0.8 will apply also at this stress ratio.

Incorporating data presented previously [4][5], FCG rates for HCF+LCF cycles at three stress ratios and four overload ratios may be collated.

At all three stress ratios the effect of overloads is to retard FCG rates, Figures 11, 12 and 13, as expected. Also the value of ΔK_{onset}, where the polynomial curves representing FCG rates for HCF+LCF intersect the LCF only cycles data increases with increasing overload. In general the curves representing the test data are parallel. The 'bunching' of overload data from R_{HCF} = 0.8 at the larger stress intensity ranges [5] and Figure 12 is not noticeable at R_{HCF} = 0.7.

If the FCG rate curves are rearranged in terms of stress ratio, Figures 14 to 17 are produced. These clearly illustrate that as the stress ratio approaches unity, the HCF+LCF FCG rates converges to the FCG rate for LCF only cycles. This is in line with expectations.

3.2 Onset

The intersection of the HCF polynomial curve with the LCF only curve is termed 'onset'; which may be considered as the point at which crack growth due to HCF cycles begins to contribute to the overall crack growth. With the polynomial equations which were used to construct Figures 11 to 13, Table 4 may be assembled from which characteristics may be deduced.

Table 4 Experimental values of ΔK_{onset} (MPa$\sqrt{}$ m). Established from Figures 11 to 13.

Stress Ratio	Overload Ratio, T			
	SUC 1.0	SOC 1.15	SOC 1.3	SOC 1.45
0.7	9.7	10.8	12.2	13
0.8	12.6	12.9	14.2	15.3
0.9	15.1		18.2	

Introducing overloads into fatigue cycles clearly retards the start of HCF damage, where HCF and LCF cycles are conjoint. The implication is that thereby a useful increase in life is obtained.

3.3 Threshold

The fatigue threshold values have been determined for SUC at stress ratios, R_{HCF} = 0.7 and 0.9 using the jump-in, or step-change, method. Experimental values for the stress ratio of 0.8 have been presented previously, [5] but with more stress ratios available, the analysis of the data has been refined for all stress ratios and those for R=0.8 are included for comparison with the new data. The results are presented in Table 5.

Table 5 Experimental values of ΔK_{th} by the jump-in, or step-change, method.

Stress Ratio	Maximum ΔK_{th} MPa$\sqrt{}$m	Minimum ΔK_{th} MPa$\sqrt{}$m	Mean ΔK_{th} MPa$\sqrt{}$m
0.7	3.24	2.73	**2.98**
0.8	2.66	2.22	**2.44**
0.9	2.15	1.93	**2.04**

A difference between maximum and minimum values of ΔK_{th} is expected both from the method of determining threshold and from scatter in the test results. It is convenient to quote one value of ΔK_{th}, the mean of the difference fulfilling that role. The mean values clearly demonstrate the decrease in threshold value as the stress ratio increases. Threshold values at comparable stress ratios for Ti-6Al-4V forged material have been found previously [6][7]. These, along with the current values of ΔK_{th} are presented as Figure 18. The values of ΔK_{th} determined from the current test results agree closely with the results of Powell and Hopkins et al.

4. DISCUSSION

Results from the new tests at intermediate overload ratios of 1.15 and 1.45 at the stress ratio of 0.7 confirms the initial findings [4] and shows that the application of overloads has a similar effect as for a stress ratio of 0.8. As is to be expected, the larger HCF stress range for the stress ratio of 0.7 results in greater FCG rates as indicated by the greater FCG rates from HCF+LCF loading blocks at this stress ratio than at 0.8. This implies that overloads have a greater effect in terms of numerical values, but the effect is in proportion to the stress ratio.

Results from the two sets of test data for a stress ratio of 0.9 support the trends deduced from the results from stress ratios of 0.7 and 0.8. FCG rates at R_{HCF}=0.9 being less at a given stress intensity range than for smaller stress ratios, the effect of overloads in reducing FCG rates being in proportion.

The similarity in the effects of overloads on FCG rates is clearly illustrated in the collective diagrams, Figures 11 to 13, with an increase in overload ratio reducing the HCF+LCF FCG rate towards the LCF only FCG rate. This infers that there is an overload ratio at which the effect of overload completely negates the HCF contribution to HCF+LCF FCG rate. Part of the proposed work for Phase IV of this

project is to investigate where this overload ratio might occur. Although not proven, the diagrams appear to suggest that the relationship between overload ratio and reduction of FCG rate is not linear and the further investigation may clarify the situation.

The increase in ΔK_{onset} with increasing overload, which is evident in Table 4, is in line with the findings of others [8] and conforms to the relationship that ΔK_{onset} increases with increasing stress ratio. However there is not enough data in Table 4 to determine whether there is any influence of overloads on the effect of stress ratio on the value of ΔK_{onset}.

Equation (1) can be used to relate ΔK_{th} to ΔK_{onset} by the relationship :-

$$\mathbf{\Delta K_{HCFonset} = \Delta K_{LCFonset} (1 - R_{HCF}) / (1 - R_{LCF})} \qquad \mathbf{.....(2)}$$

Where $\Delta K_{th} = \Delta K_{HCFonset.}$

Applying equation (2) with the values of ΔK_{onset} for SUC in Table 4, the 'derived from onset' values for ΔK_{th} in Table 6 are obtained. Values of ΔK_{th} from Powell [6], who used the load-shed method for determining threshold, have been included in the table.

Table 6 Values of ΔK_{th} from three sources.

Stress Ratio R_{HCF}	Source of ΔK_{th} (MPa$\sqrt{m}$)		
	Experimental	**Derived from onset**	**Powell [6]**
0.7	2.98	2.94	
0.75			2.96
0.8	2.44	2.54	
0.82			2.21
0.9	2.04	1.52	2.12

Applying equation (2) to onset values where overloads have been applied results in the value of ΔK_{th} increasing as the magnitude of the overload increases. In modification of earlier findings [5] recalculation and reassessment of the threshold data for this report indicates that further investigation may be desirable. If no increase in ΔK_{th} occurs on the application of overload, then equation 2 must be modified to accommodate that fact. Work is currently in progress to clarify the situation.

5. CONCLUSIONS

Fatigue crack growth rates have been measured in Ti-6Al-4V at room temperature. HCF loadings with a stress ratio of 0.7 and 0.9 and LCF loadings with a stress ratio of 0.01 have been applied in various combinations.

For all three stress ratios the effect of applying overloads on HCF+LCF cycles is to reduce the influence of the HCF cycles on crack growth and increase the stress intensity range at which the HCF cycles become active.

The jump-in threshold values have been determined, without overload, for the three stress ratios of 0.7, 0.8 and 0.9 are 3.0, 2.4 and 2.0 MPa$\sqrt{m}$ respectively.

REFERENCES

1 ASTM Standard E-399-90, 1990, *03.01*, 407

2 Hicks, M. A. and Pickard, A. C. *Int. J. of Fract.* 1980, *20*, 91

3 Pickard, A. C. *The Application of 3-Dimensional Finite Element Methods to Fracture Mechanics and Fatigue Life Predictions* EMAS, Warley, UK.1986.

4 Hall R.F., Powell, B.E. & Byrne, J. *US AFSOR study report; Interim Report for Phase III*, F568, November 1999.

5 Hall R.F., & Powell, B.E. *US AFSOR study report; Final Report for Phase II*, F567, May1999.

6 Powell, B. E. "The influence of minor cycles on low cycle fatigue crack propagation", *PhD Thesis*, University of Portsmouth 1985.

7 Hopkins, S. W. Rau, C. A. Leverant, G. R. and Yuen, A. "Effects of various programmed overloads on the threshold for high-frequency fatigue crack growth. "*ASTM STP 595,* 1976, 125

8 Moshier, M.A. Nicholas, T. and Hillberry, B.M. "The effect of low cycle fatigue cracks and loading history on low cycle fatigue threshold" Cape Cod conf. Sept. 2000

FIGURES

Figure 1 Schematic representation of the repeated stress - time sequences used in the tests considered in this report. a) Single Underload Cycle; b) Multiple Underload Cycle; c) Single Overload Cycle; d) Multiple Overload Cycle.

Figure 2 Schematic representation of the stress - time sequences used in the jump-in threshold tests. a) Overload ratio, (T) = 1.0; b) Overload ratio, (T) = 1.3.

Figure 3 Experimental FCG rate data for two SOC tests at R_{HCF}=0.7. Overload ratio = 1.15; cycle ratio = 1000:1. LCF data curve included.

Figure 4 Polynomial fit to the SOC experimental data in Figure 3. Onset at ΔK_{LCF} = 10.8 MPa$\sqrt{m}$. Data for R_{HCF} = 0.7; T = 1.15; n = 1000:1.

Figure 5 Experimental FCG rate data for two SOC tests at R_{HCF}=0.7. Overload ratio = 1.45; cycle ratio = 1000:1. LCF data curve included.

Figure 6 Polynomial fit to the SOC experimental data in Figure 5. Onset at ΔK_{LCF} = 13.0 MPa$\sqrt{m}$. Data for R_{HCF} = 0.7; T = 1.45; n = 1000:1.

Figure 7 Experimental FCG rate data for two SOC tests at R_{HCF}=0.9. Overload ratio = 1.0; cycle ratio = 1000:1. LCF data curve included.

Figure 8 Polynomial fit to the SOC experimental data in Figure 7. Onset at ΔK_{LCF} = 15.1 MPa$\sqrt{m}$. Data for R_{HCF} = 0.9; T = 1.0; n = 1000:1.

Figure 9 Experimental FCG rate data for two SOC tests at R_{HCF}=0.9. Overload ratio = 1.3; cycle ratio = 1000:1. LCF data curve included.

Figure 10 Polynomial fit to the SOC experimental data in Figure 9. Onset at ΔK_{LCF} = 18.2 MPa$\sqrt{m}$. Data for R_{HCF} = 0.9; T = 1.3; n = 1000:1.

Figure 11 Experimental FCG rate data from Single Underload and Single Overload tests at R_{HCF} = 0.7. Cycle ratio = 1000:1.

Figure 12 Experimental FCG rate data from Single Underload and Single Overload tests at R_{HCF} = 0.8. Cycle ratio = 1000:1.

Figure 13 Experimental FCG rate data from Single Underload and Single Overload tests at R_{HCF} = 0.9. Cycle ratio = 1000:1.

Figure 14 Experimental FCG rate data from Single Underload Cycle tests. Overload ratio, T = 1.0. Cycle ratio = 1000:1.

Figure 15 Experimental FCG rate data from Single Overload Cycle tests. Overload ratio, T = 1.15. Cycle ratio = 1000:1.

Figure 16 Experimental FCG rate data from Single Overload Cycle tests. Overload ratio, T = 1.3. Cycle ratio = 1000:1.

Figure 17 Experimental FCG rate data from Single Overload Cycle tests. Overload ratio, T = 1.45. Cycle ratio = 1000:1.

Figure 18 Experimental fatigue threshold values as a function of stress ratio for Ti-6Al-4V forged material. Room temperature tests. A comparison of data from three sources.

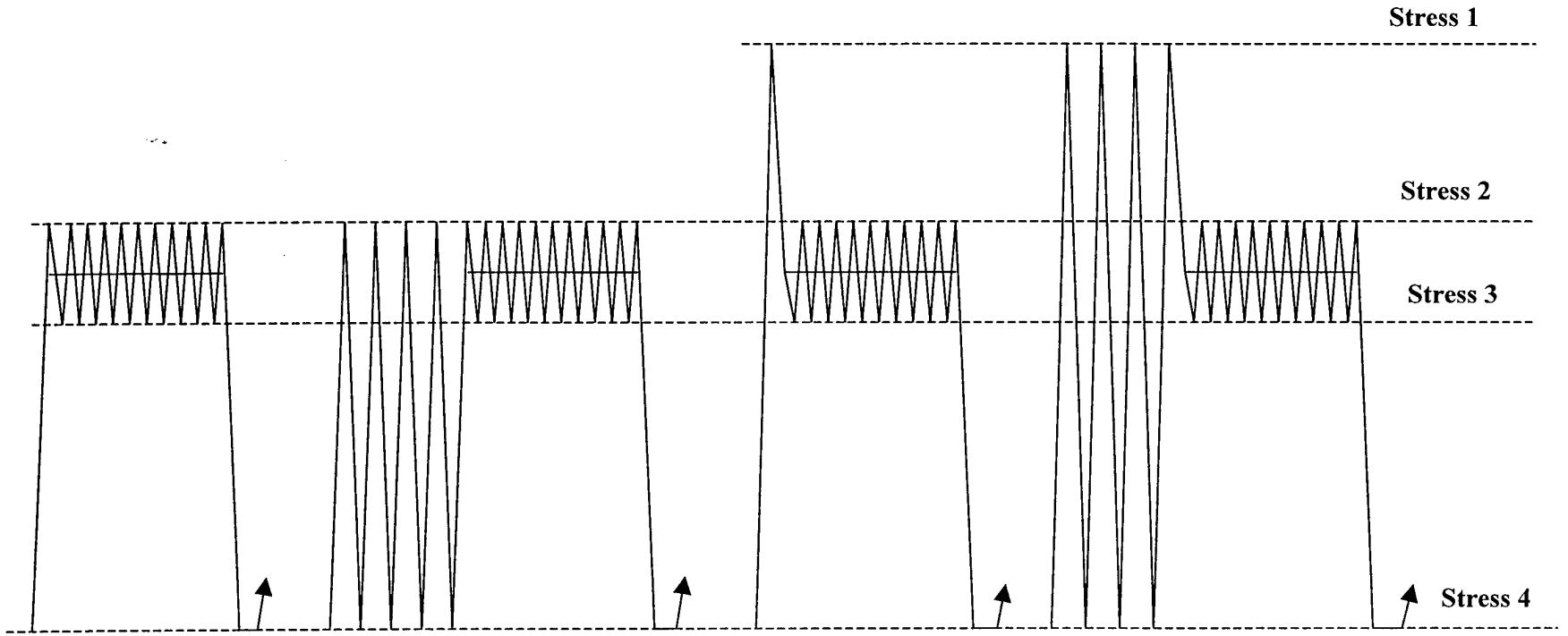

Figure 1. Schematic representation of the repeated stress – time sequences used in the tests.
(a) Single Underload Cycle; (b) Multiple Underload Cycles;
(c) Single Overload Cycle; (d) Multiple Overload Cycles.

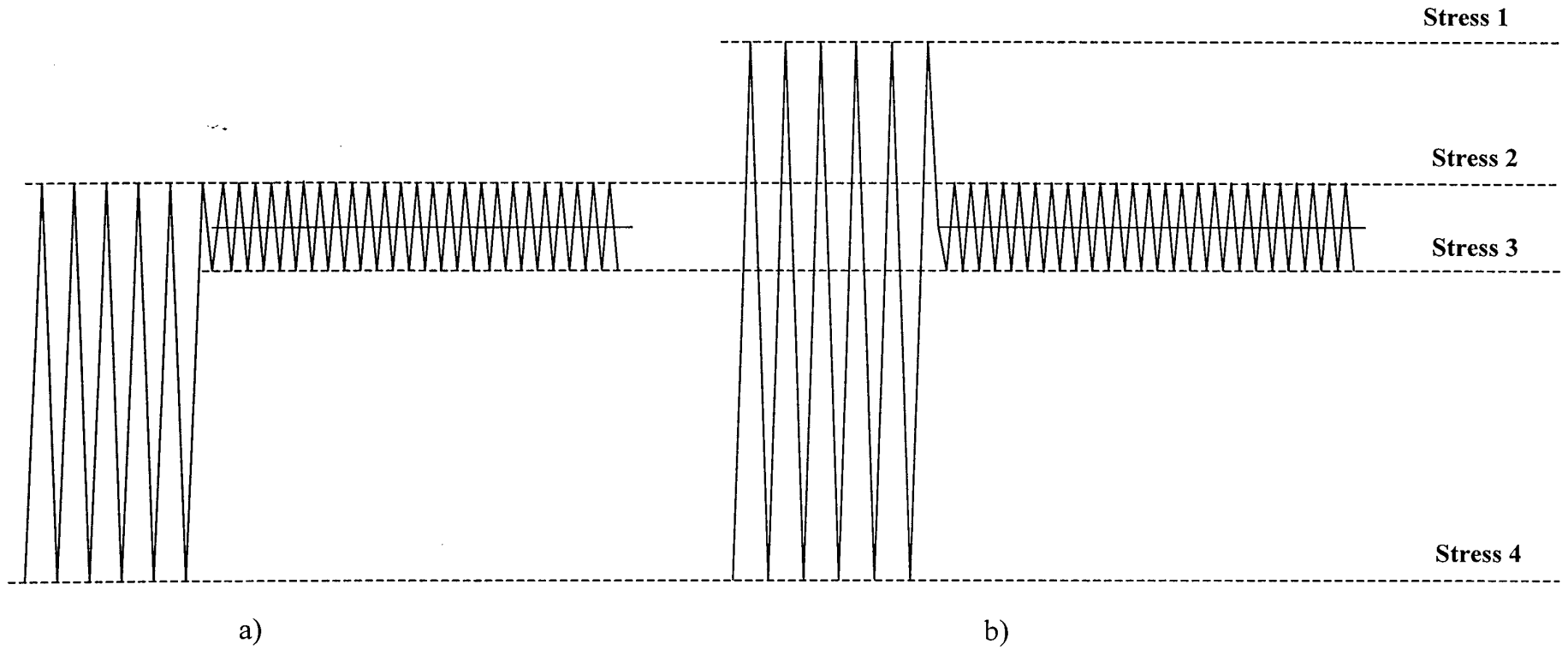

Figure 2. Schematic representation of the stress – time sequences used in the jump-in threshold tests.
(a) Without overload: (b) With overload

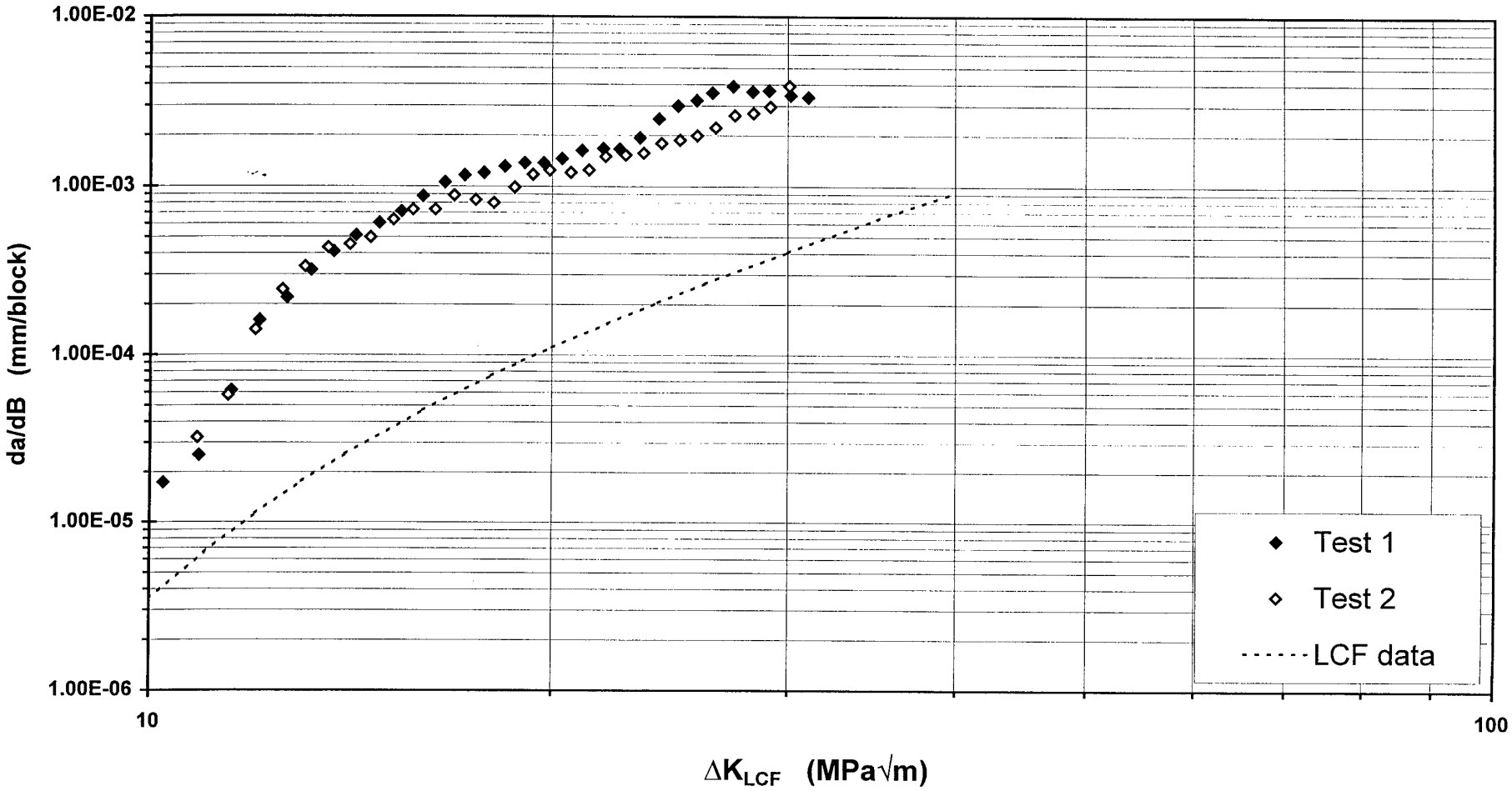

Figure 3 Experimental FCG rate data for two SOC tests at R_{HCF}= 0.7. Overload ratio = 1.15; cycle ratio = 1000:1. LCF data curve included.

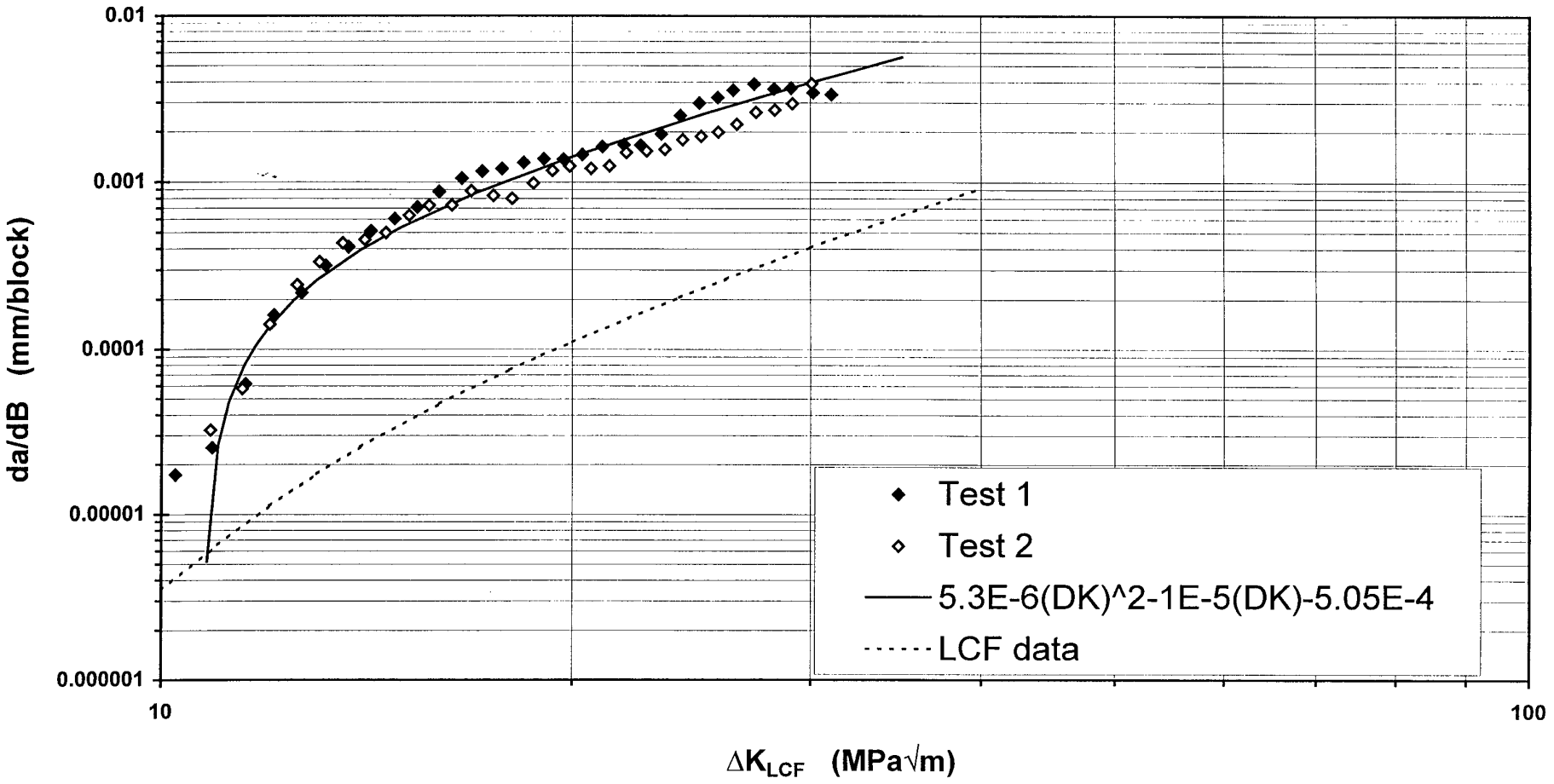

Figure 4 Polynomial fit to the SOC experimental data in Figure 3. Onset at ΔK_{LCF} = 10.8 MPa√m. Data for R_{HCF}=0.7; T=1.15; n=1000:1.

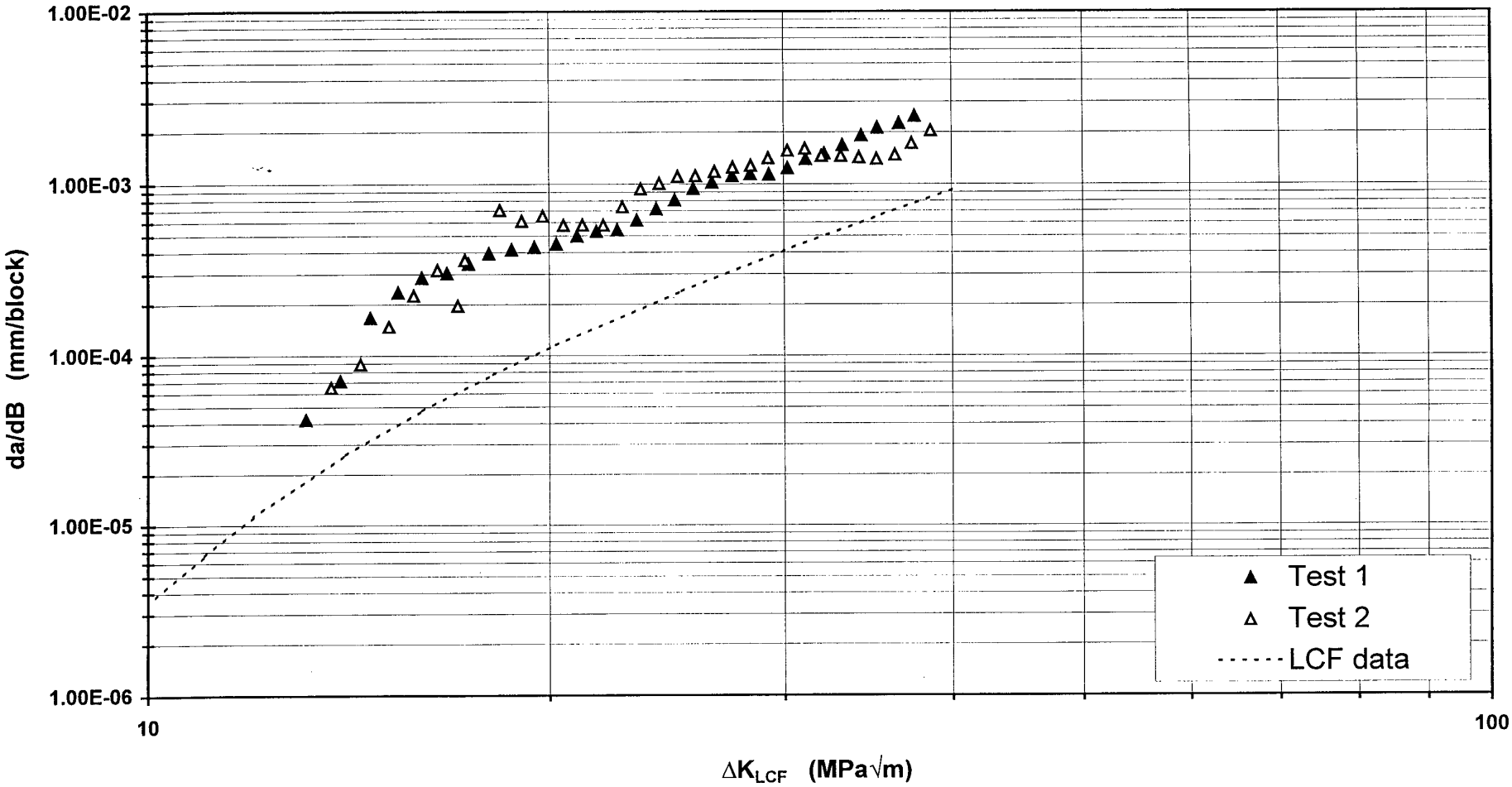

Figure 5 Experimental FCG rate data for two SOC tests at R_{HCF}= 0.7. Overload ratio = 1.45; cycle ratio = 1000:1. LCF data curve included.

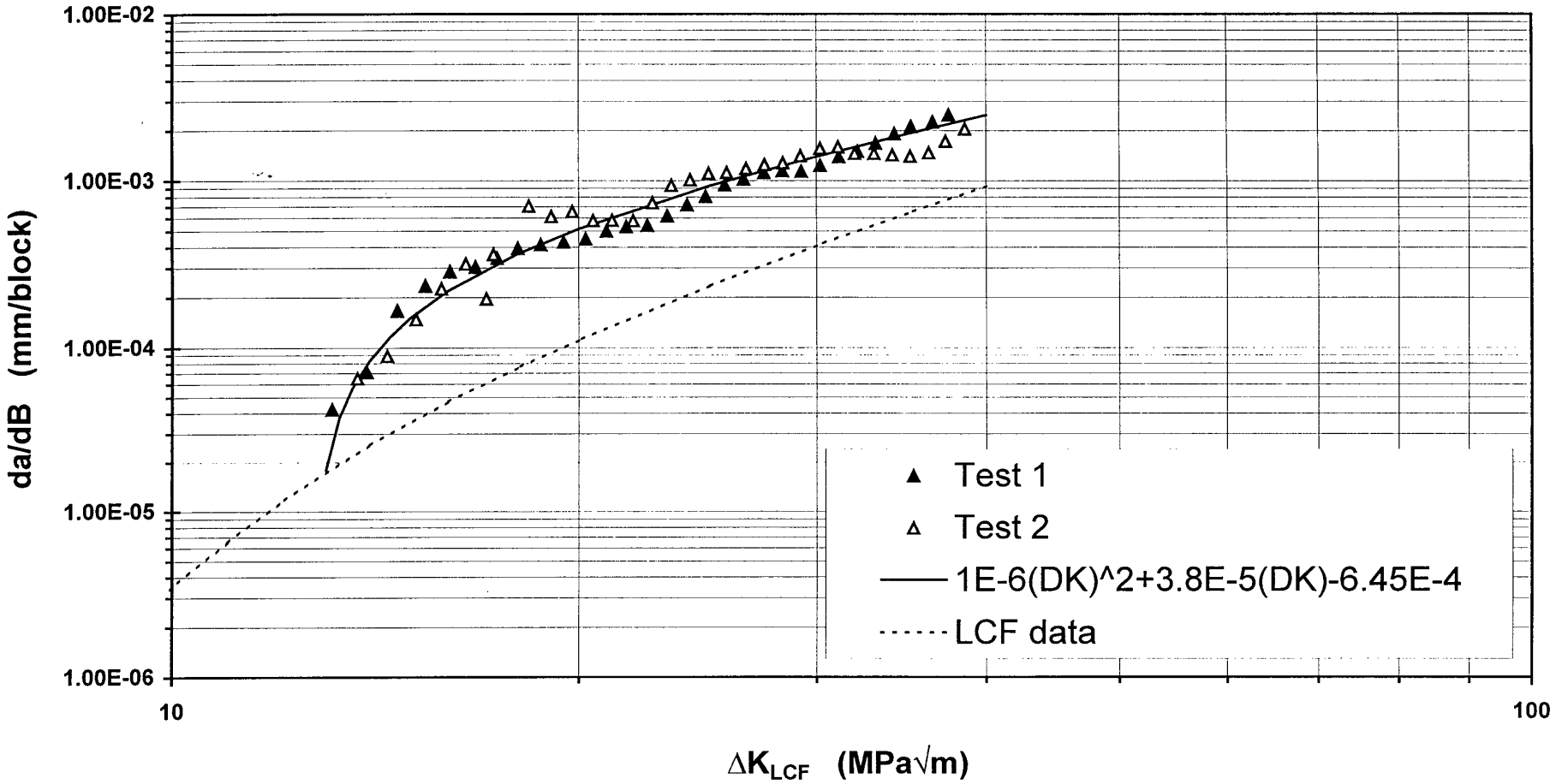

Figure 6 Polynomial fit to the SOC experimental data in Figure 5. Onset at ΔK_{LCF}=13.0MPa$\sqrt{m}$. Data for R_{HCF}=0.7; T=1.45; n=1000:1.

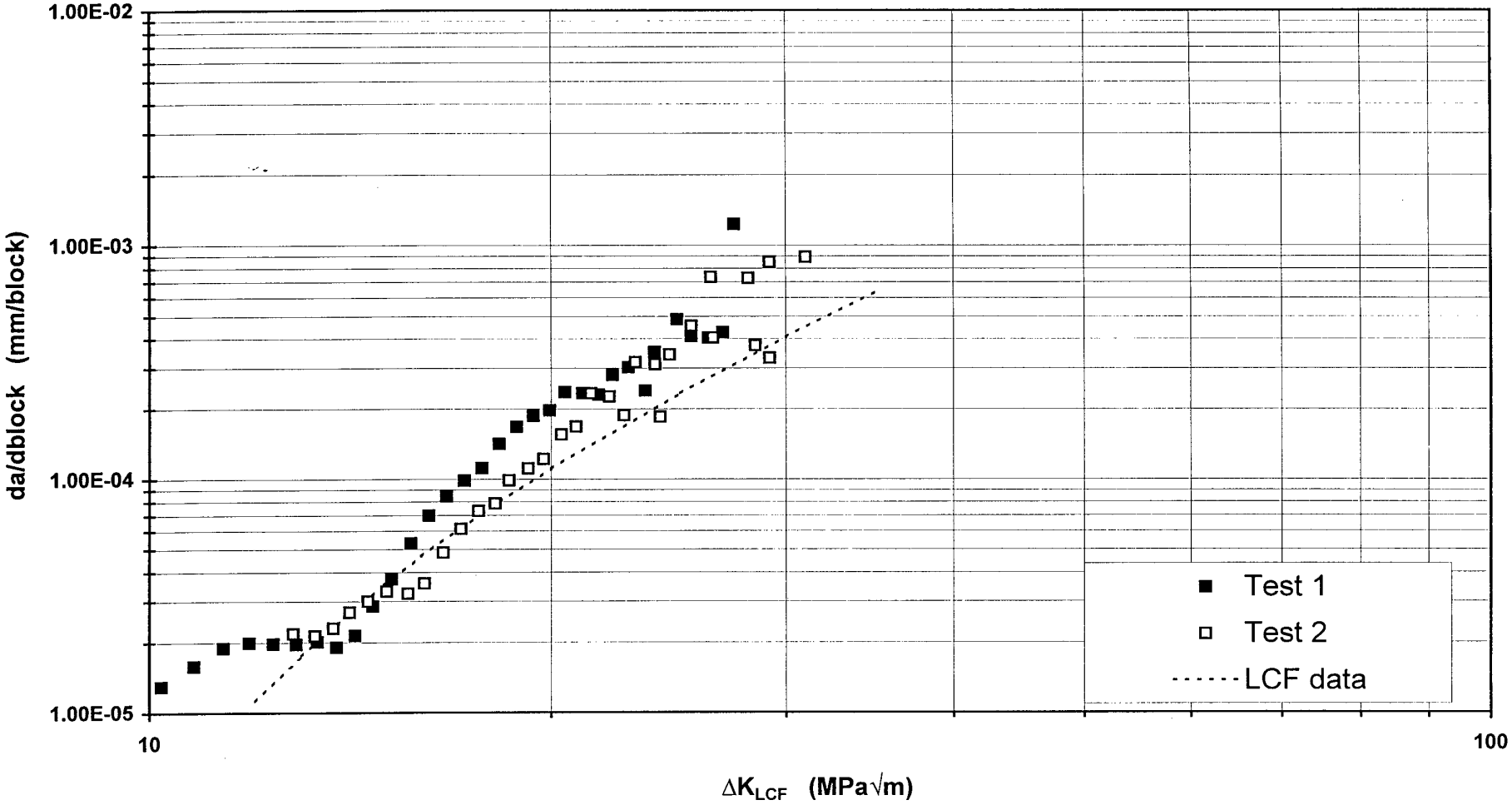

Figure 7 Experimental FCG rate data for two SUC tests at R_{HCF}=0.9. Overload ratio = 1.0; cycle ratio = 1000:1. LCF data curve added.

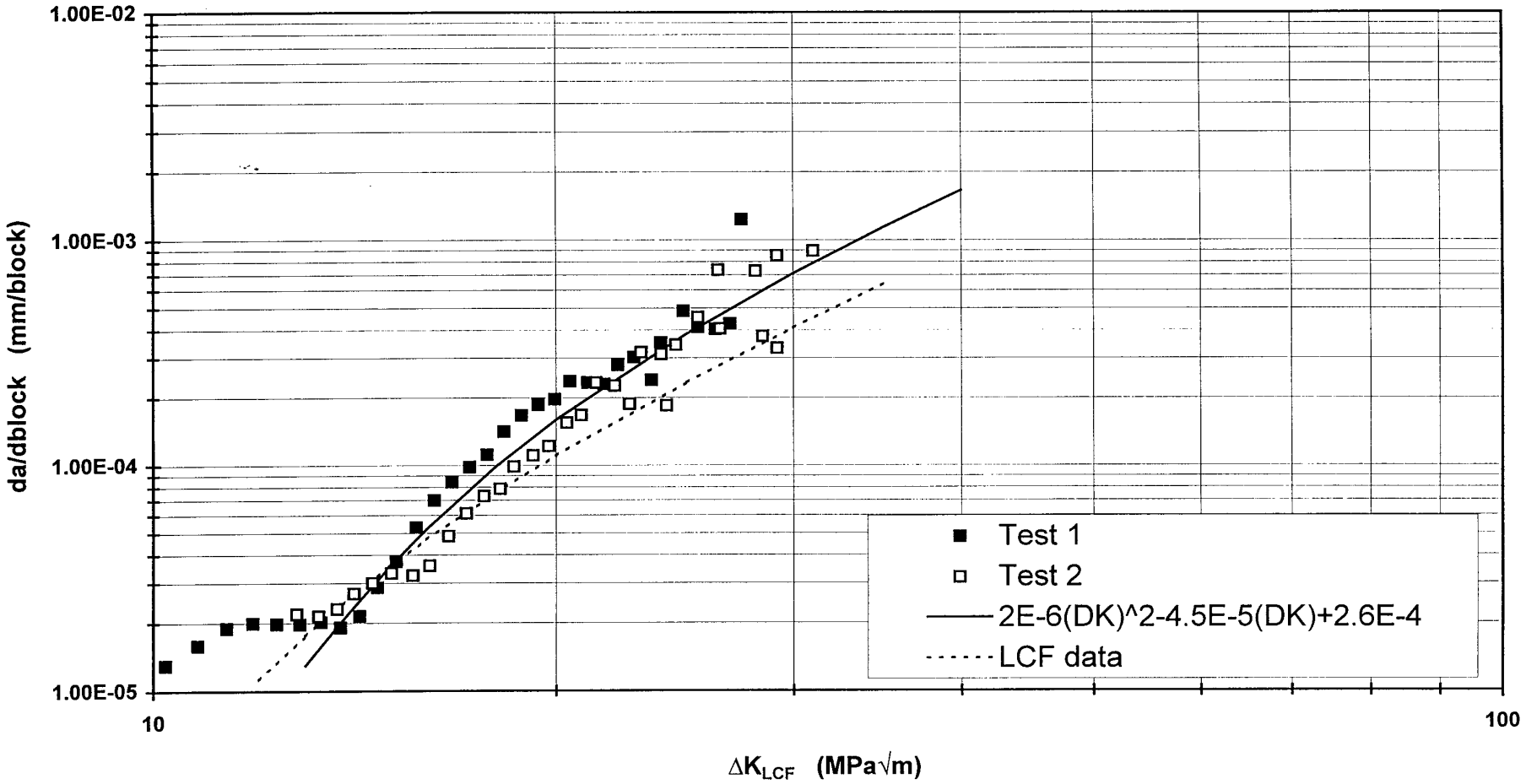

Figure 8 Polynomial fit to the SUC experimental data in Figure 7. Onset at ΔK_{LCF}=15.1 MPa√m. Data for R_{HCF}=0.9;T=1.0;n=1000:1.

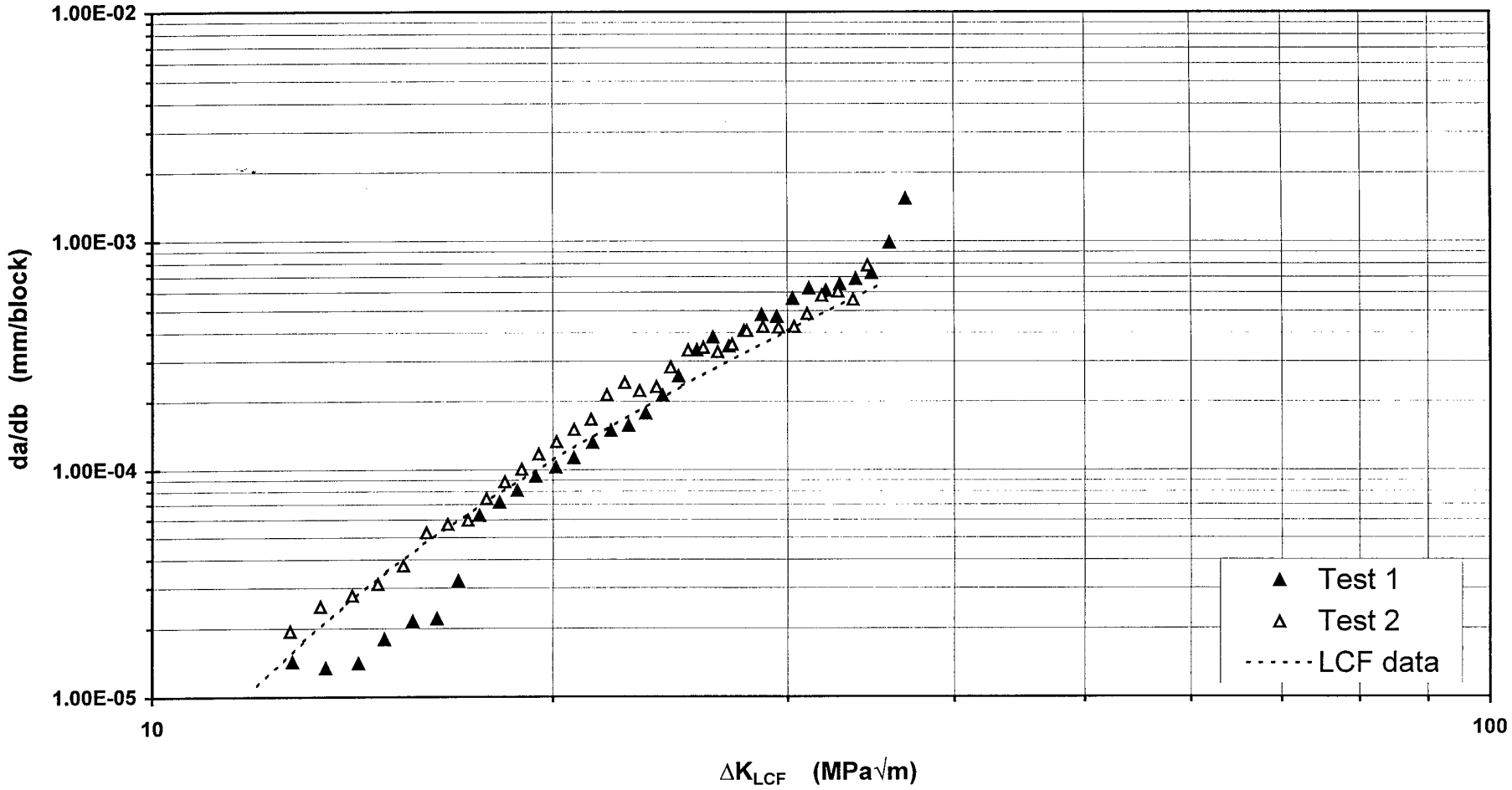

Figure 9 Experimental FCG rate data for two SOC tests at R_{HCF}=0.9. Overload ratio = 1.3; cycle ratio = 1000:1. LCF data curve added.

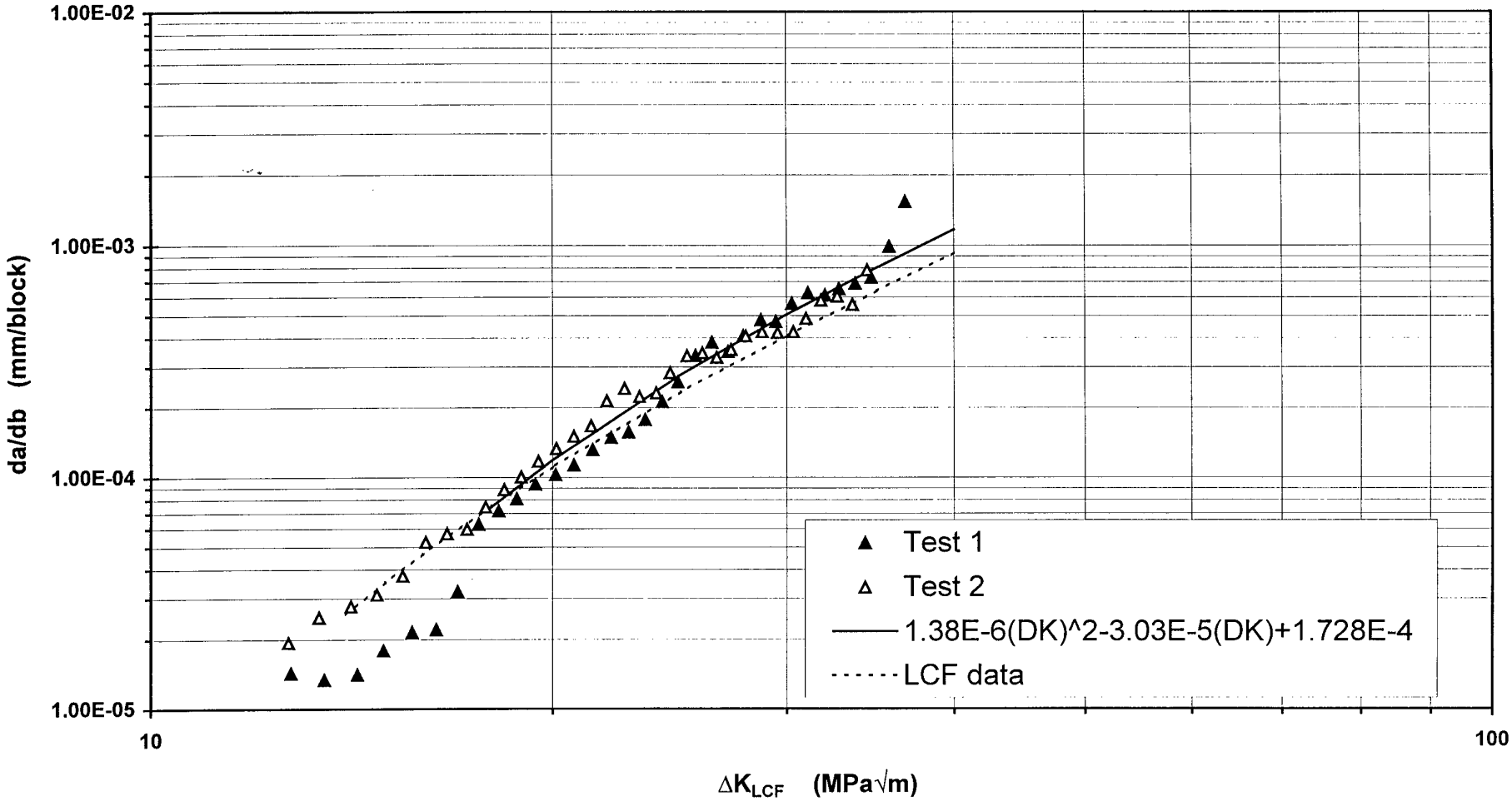

Figure 10 Polynomial fit to the SOC experimental data in Figure 9. Onset at ΔK_{LCF}=18.2 MPa$\sqrt{m}$. Data for R_{HCF}=0.9; T=1.3; n=1000:1.

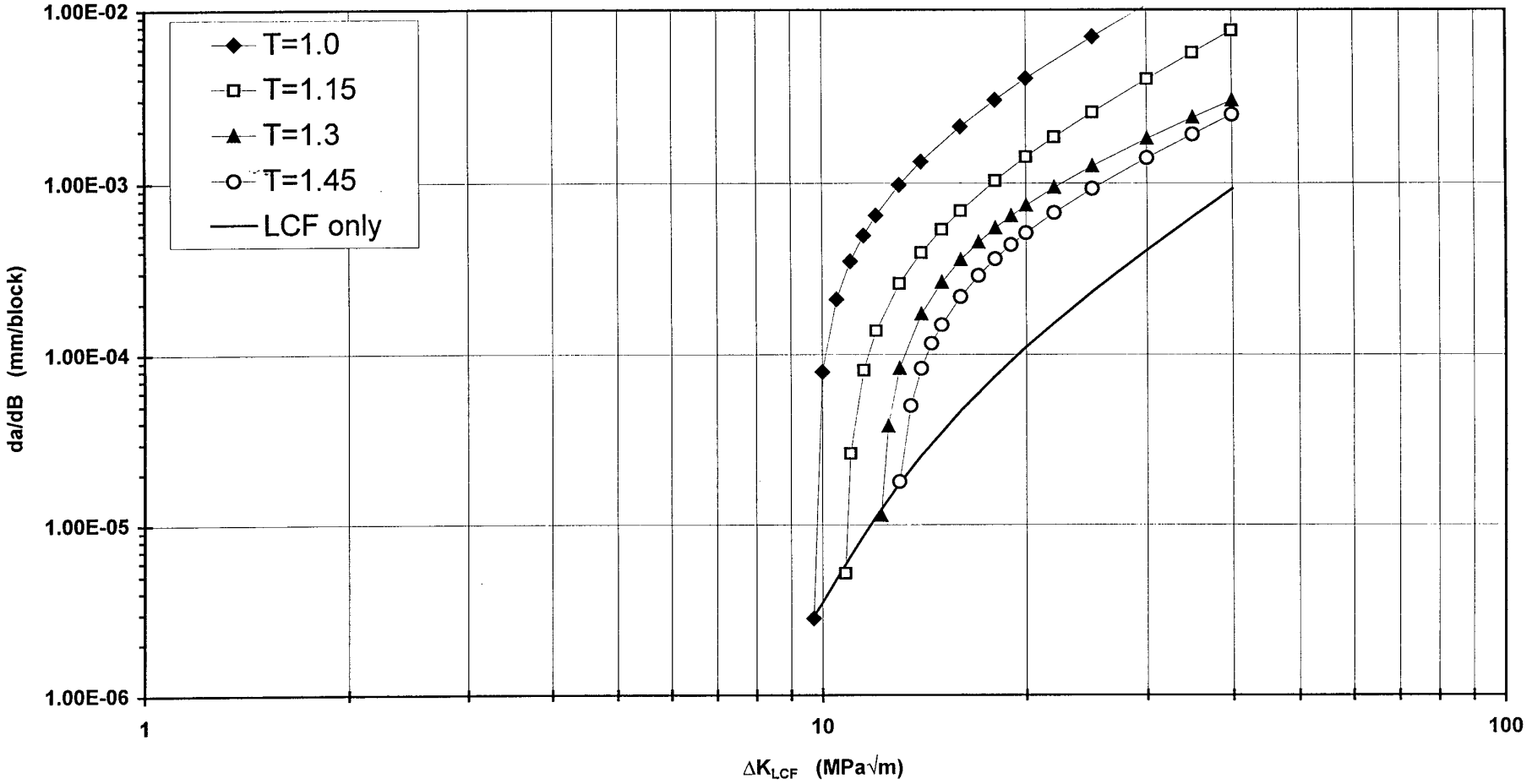

Figure 11 Experimental FCG rate data from Single Underload and Single Overload tests at R_{HCF} = 0.7. Cycle ratio = 1000:1.

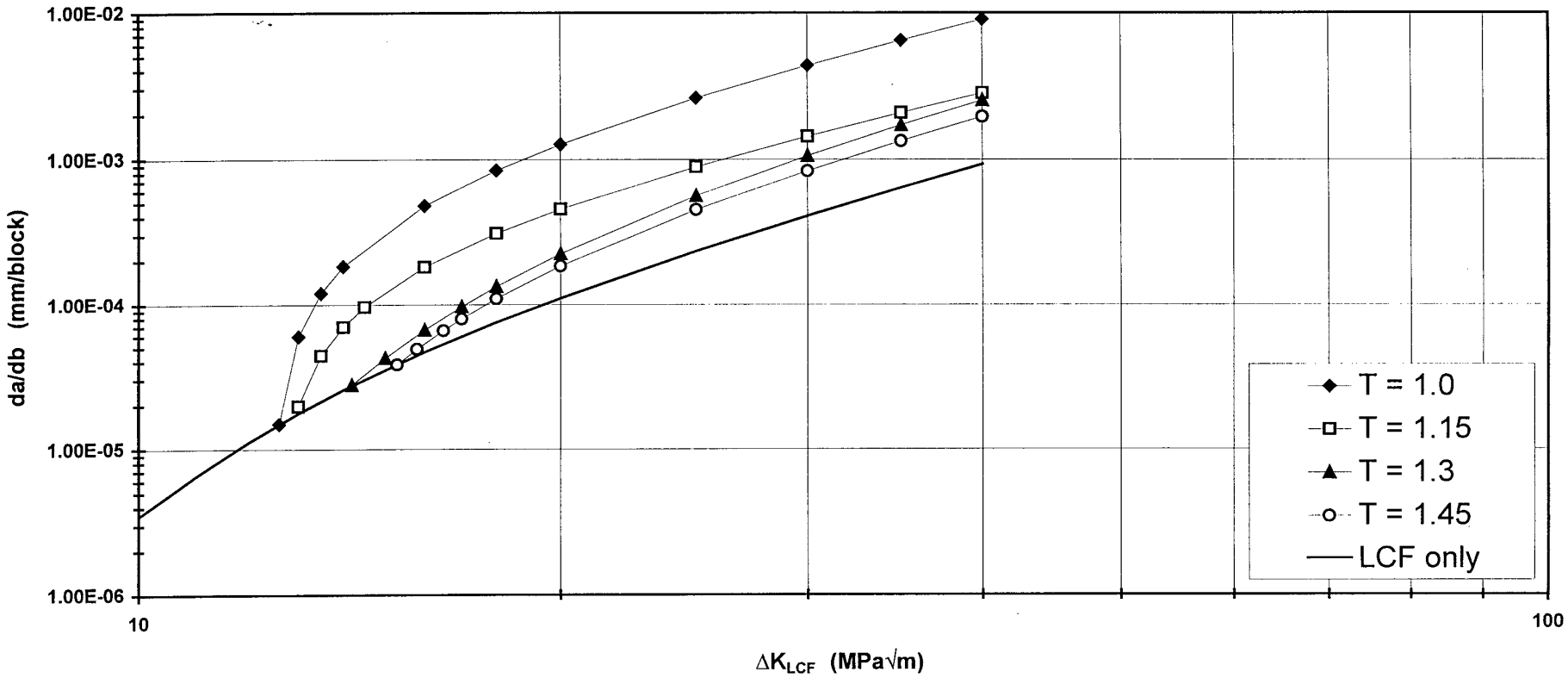

Figure 12 Experimental FCG rate data from Single Underload and Single Overload tests at R_{HCF} = 0.8. Cycle Ratio = 1000:1.

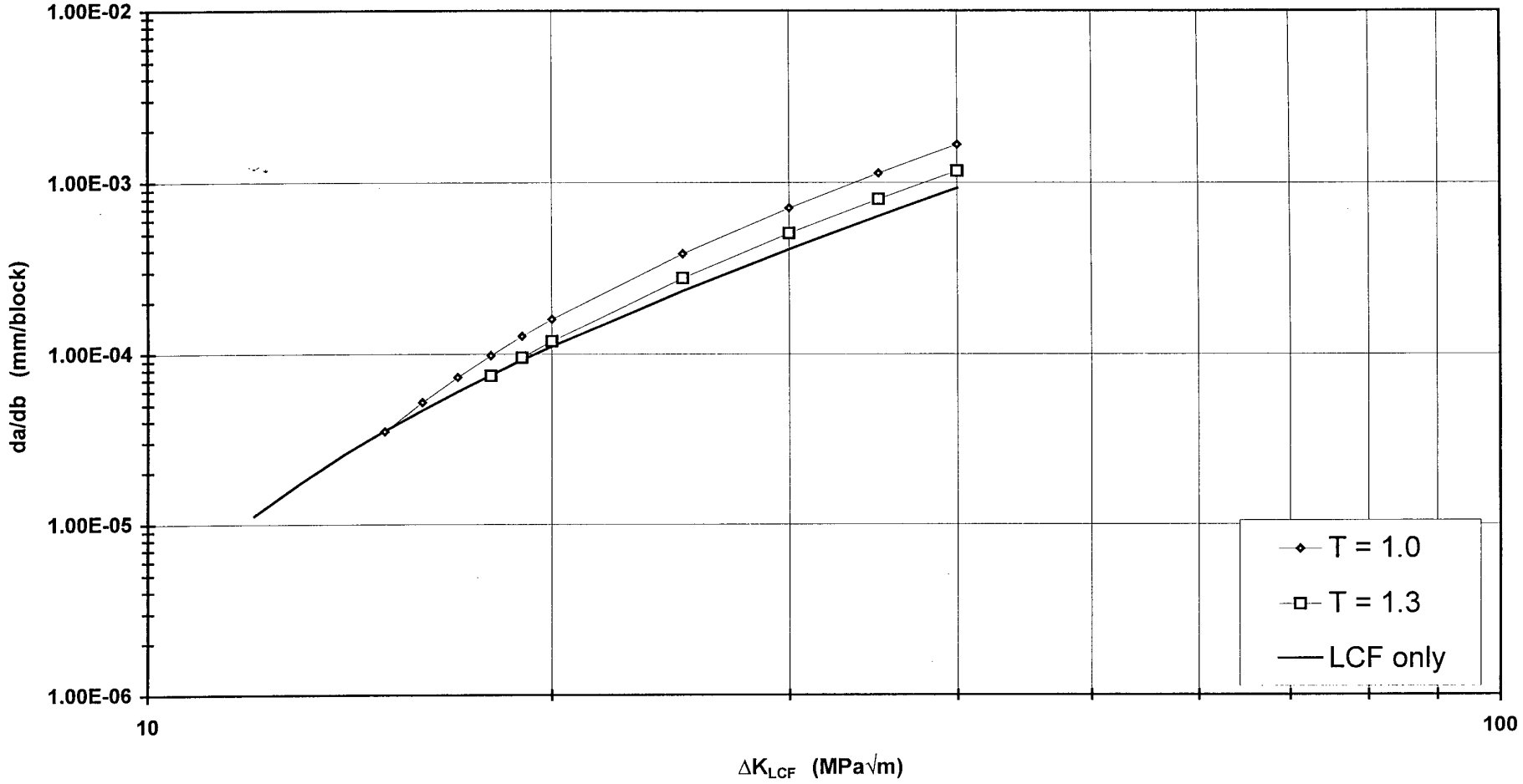

Figure 13 Experimental FCG rate data from Single Underload and Single Overload tests at R_{HCF} = 0.9. Cycle ratio = 1000:1.

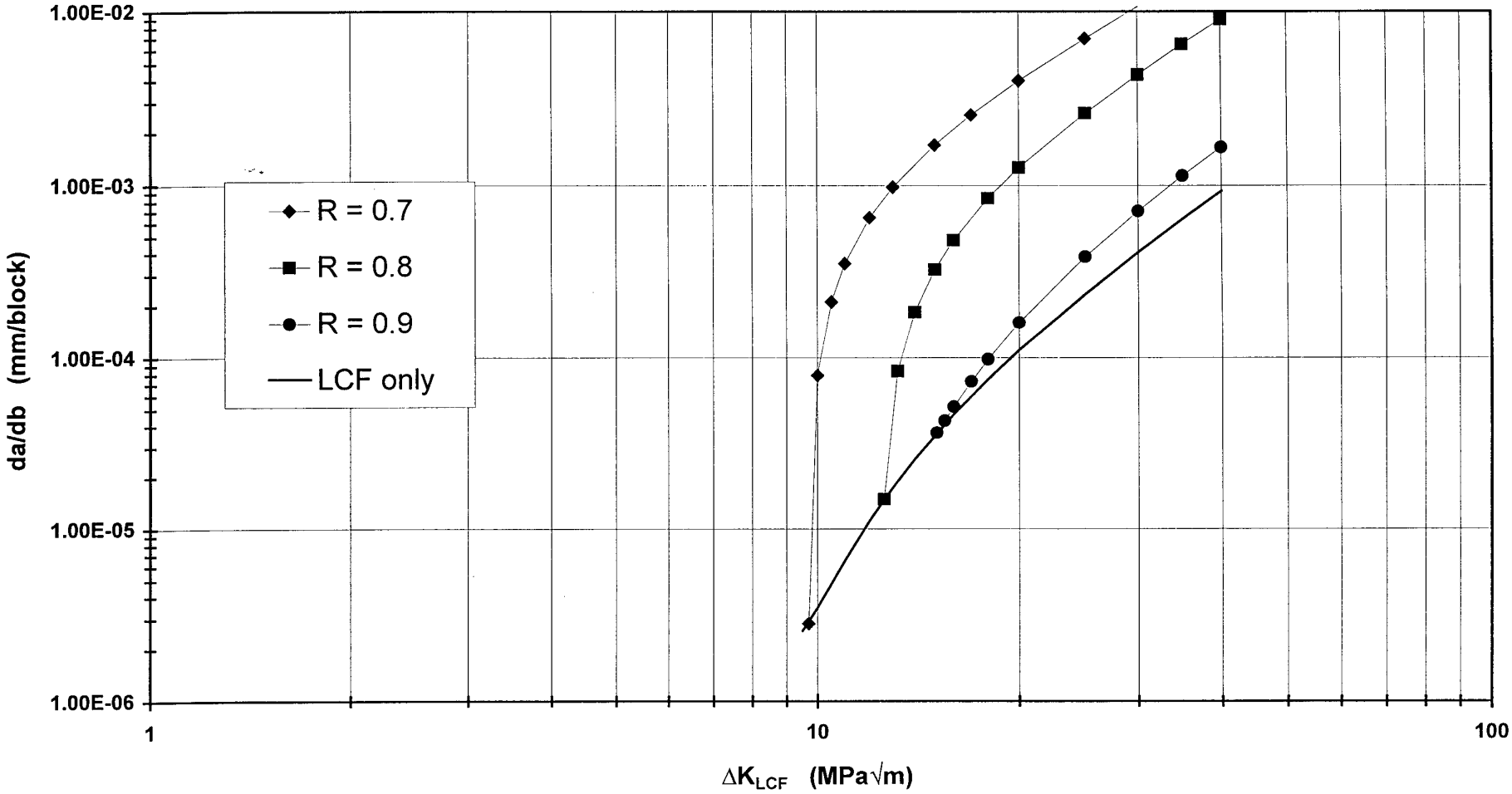

Figure 14 Experimental FCG rate data from Single Underload Cycle tests. Overload ratio, T= 1.0. Cycle ratio =1000:1.

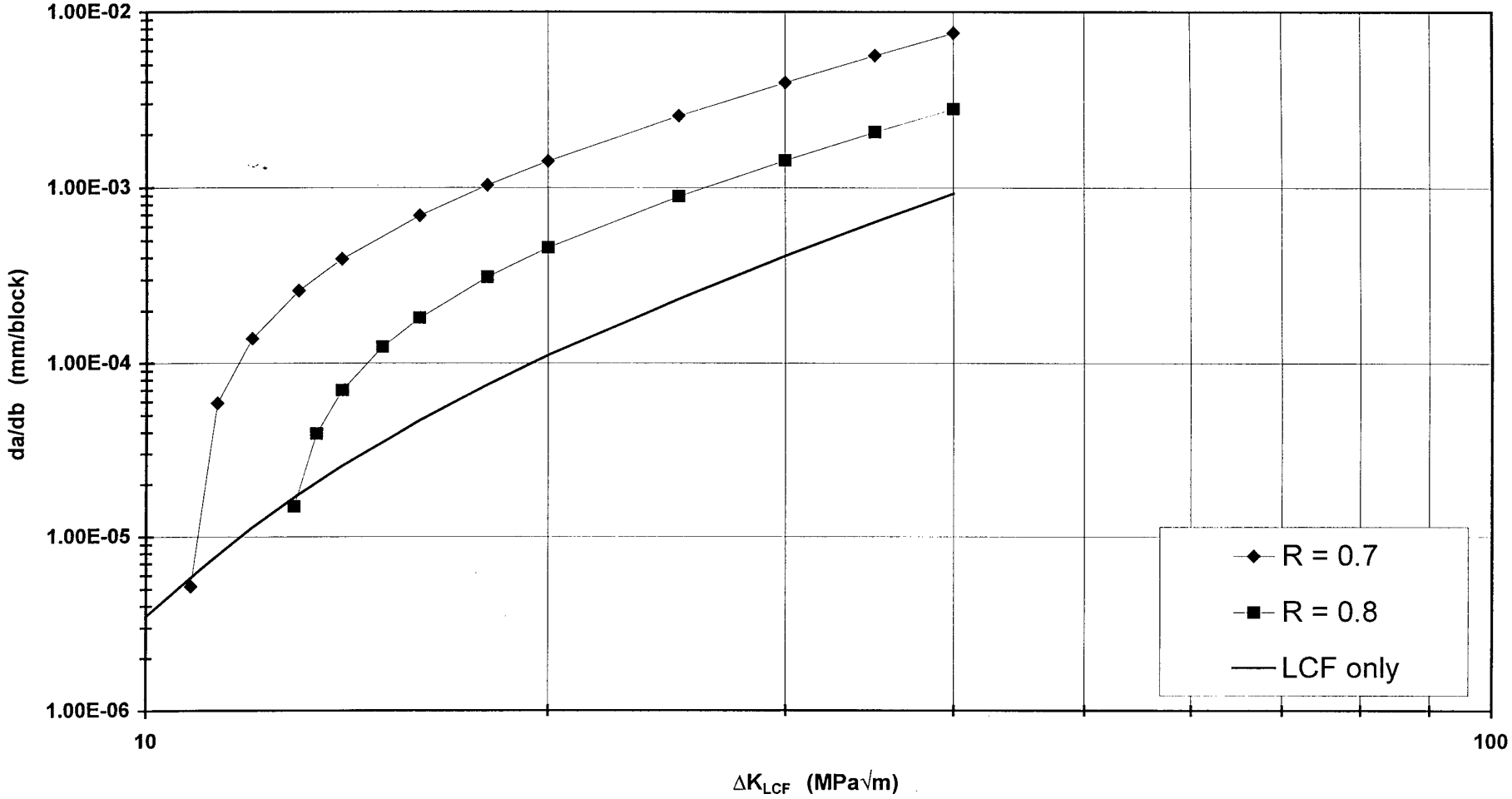

Figure 15 Experimental FCG rate data from Single Overload Cycle tests. Overload Ratio, T = 1.15; Cycle ratio = 1000:1.

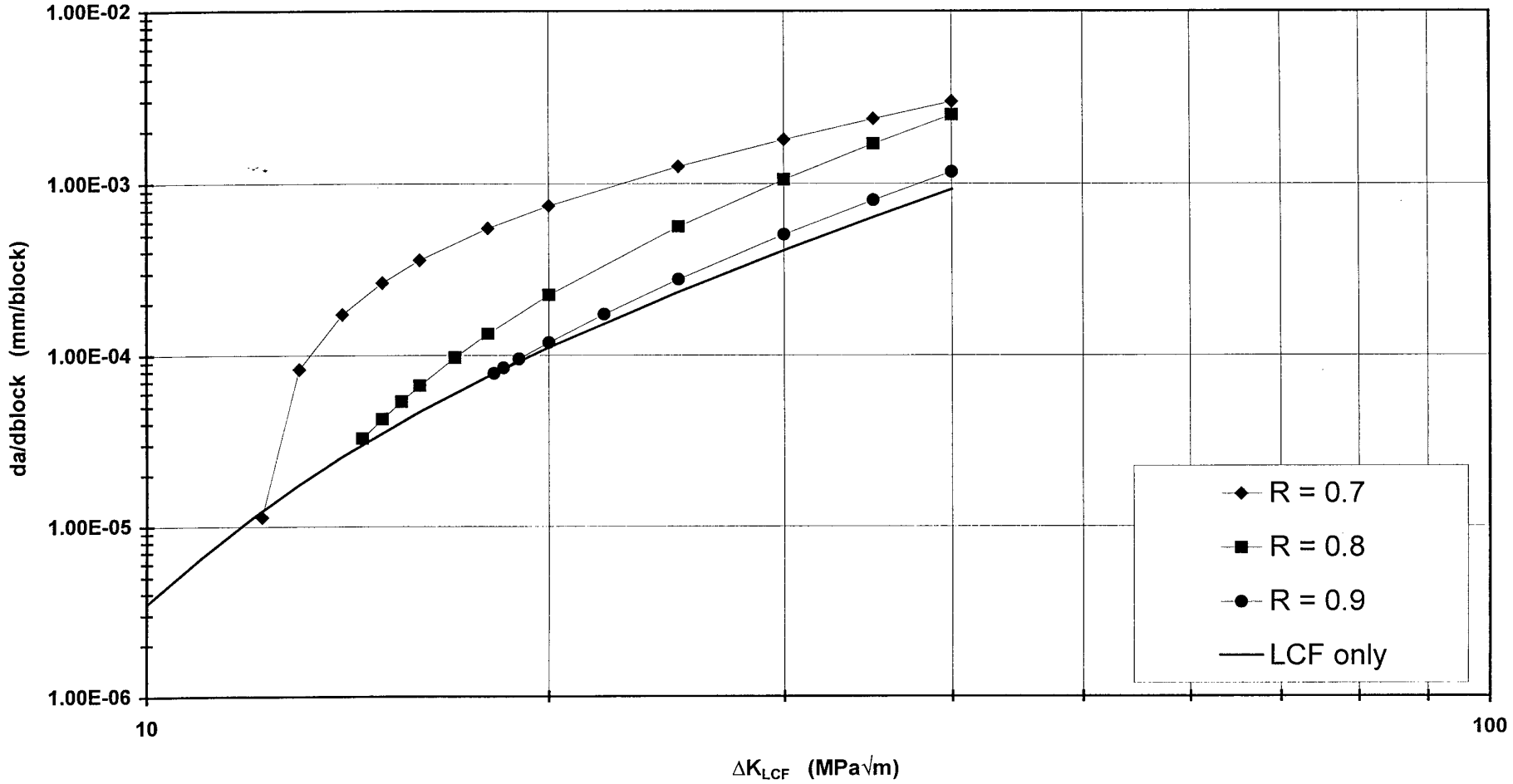

Figure 16 Experimental FCG rate data from Single Overload Cycle tests. Overload Ratio, T = 1.3. Cycle ratio = 1000:1.

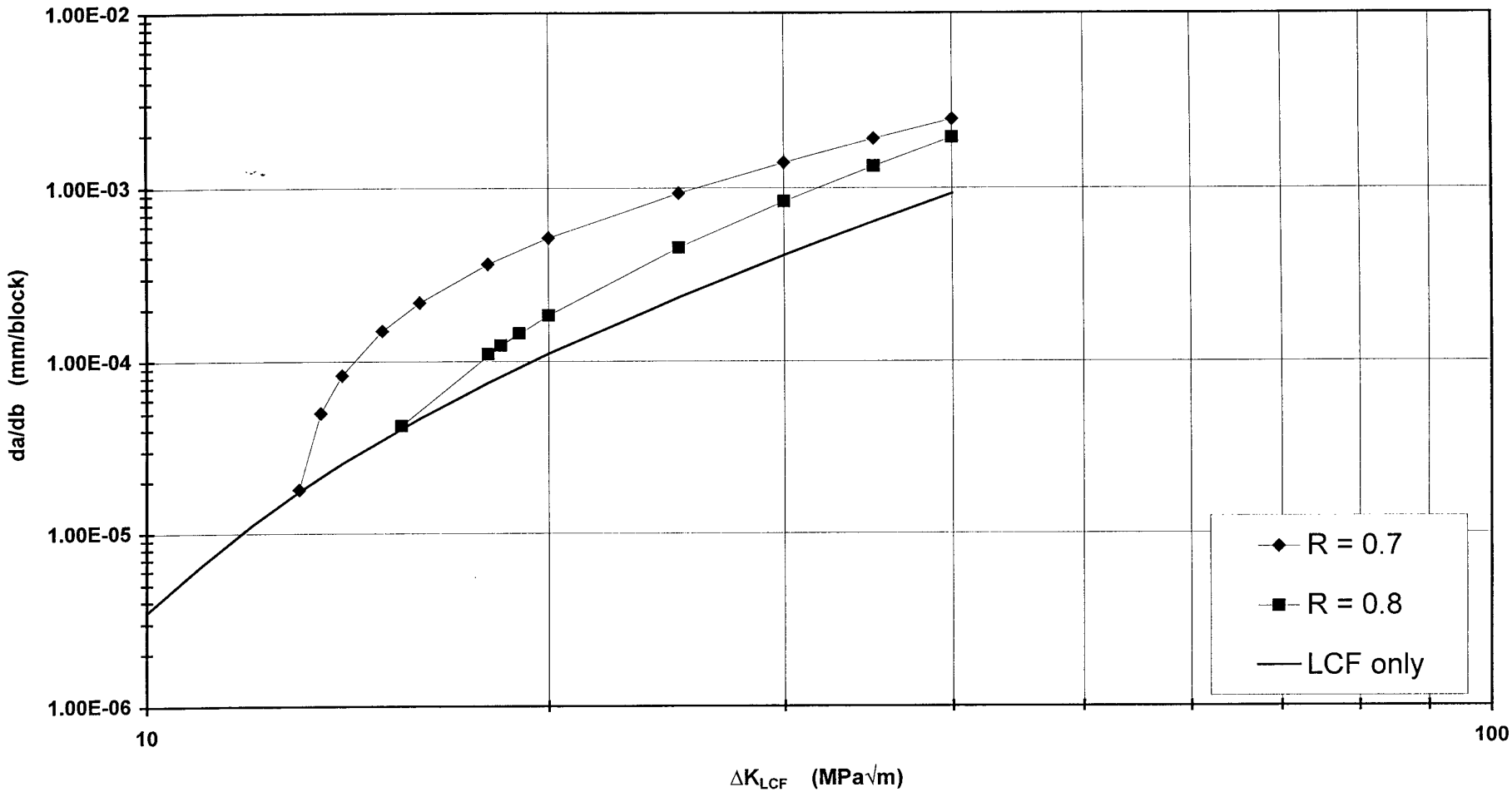

Figure 17 Experimental FCG rate data from Single Overload Cycle tests. Overload Ratio, T = 1.45; cycle ratio = 1000:1.

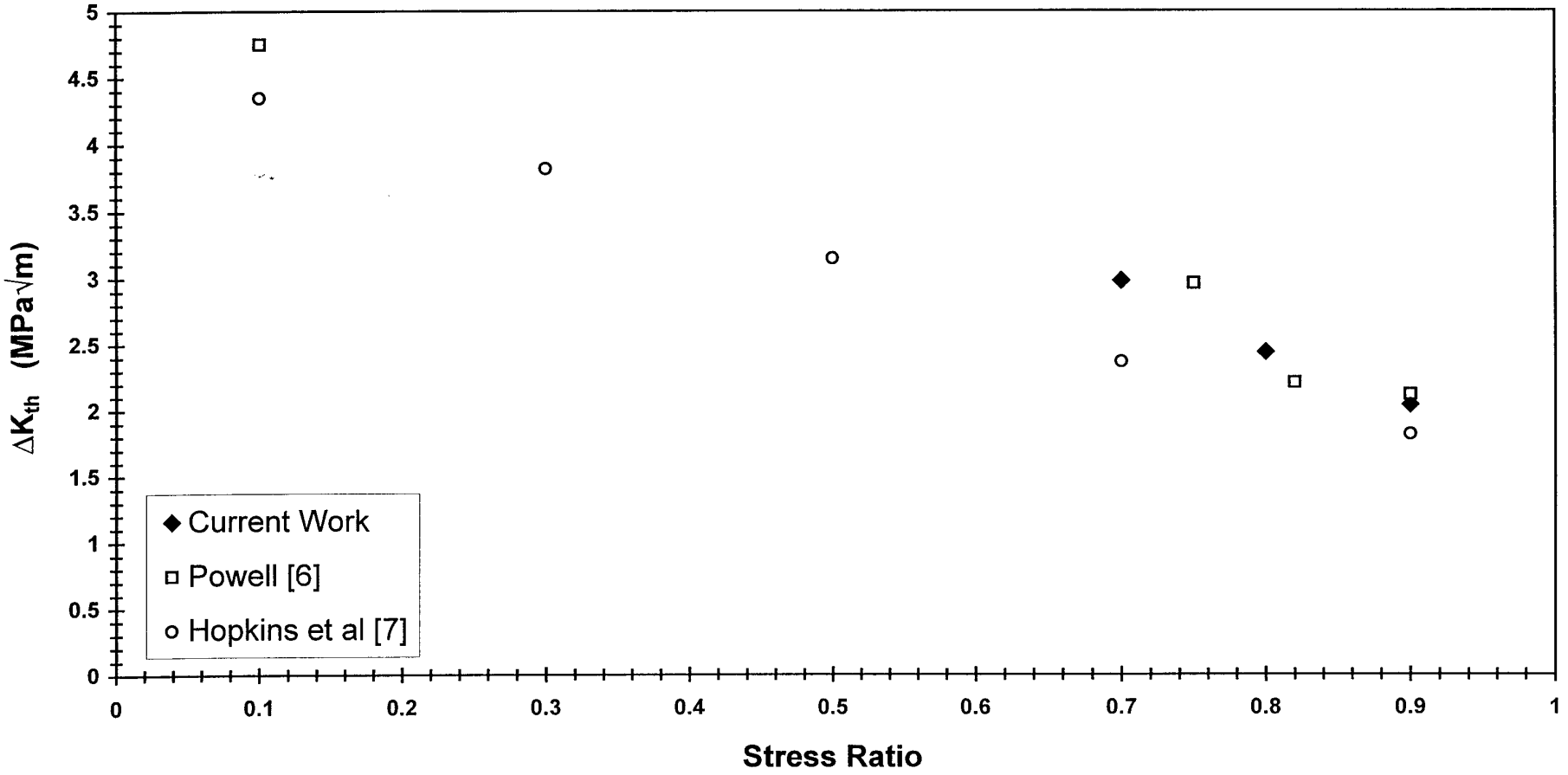

Figure 18 Experimental fatigue threshold values as a function of stress ratio for Ti-6Al-4V. Room temperature tests. A comparison of data from three sources.